JOURNAL OF GEOPHYSICAL RESEARCH, VOL. 106, NO. A12, PAGES 30,253–30,269, DECEMBER 1, 2001

Wave normal and Poynting vector calculations using the Cassini radio and plasma wave instrument

G. B. Hospodarsky, T. F. Averkamp, W. S. Kurth, and D. A. Gurnett
Department of Physics and Astronomy, University of Iowa, Iowa City, Iowa, USA

M. Dougherty
Imperial College, Blackett Laboratory, London, England

Umran Inan and Troy Wood
Department of Electrical Engineering, Stanford University, Stanford, California, USA

Abstract. Wave normal and Poynting vector measurements from the Cassini radio and plasma wave instrument (RPWS) are used to examine the propagation characteristics of various plasma waves during the Earth flyby on August 18, 1999. Using the five-channel waveform receiver (WFR), the wave normal vector is determined using the Means method for a lightning-induced whistler, equatorial chorus, and a series of low-frequency emissions observed while Cassini was in the magnetosheath. The Poynting vector for these emissions is also calculated from the five components measured by the WFR. The propagation characteristics of the lightning-induced whistler were found to be consistent with the whistler wave mode of propagation, with propagation antiparallel to the magnetic field (southward) at Cassini. The sferic associated with this whistler was observed by both Cassini and the Stanford VLF group at the Palmer Station in Antarctica. Analysis of the arrival direction of the sferic at the Palmer Station suggests that the lightning stroke is in the same sector as Cassini. Chorus was observed very close (within a few degrees) to the magnetic equator during the flyby. The chorus was found to propagate primarily away from the magnetic equator and was observed to change direction as Cassini crossed the magnetic equator. This suggests that the source region of the chorus is very near the magnetic equator. The low-frequency emission in the magnetosheath has many of the characteristics of lion roars. The average value of the angle between the wave normal vector and the local magnetic field was found to be 16°, and the emissions ranged in frequency from 0.19 to 0.75 f_{ce}, where f_{ce} is the electron cyclotron frequency. The wave normal vectors of these waves were primarily in one direction for each individual burst (either parallel or antiparallel to the local field) but varied in direction throughout the magnetosheath. This suggests that the sources of the emissions are far from the spacecraft and that there are multiple source regions.

1. Introduction

The Cassini flyby of the Earth on August 18, 1999, besides providing the necessary gravity-assist course correction, allowed the various science instruments on board to obtain measurements and perform calibrations in the reasonably well understood environment of the Earth's magnetosphere. For the Cassini radio and plasma wave science (RPWS) instrument this flyby provided an opportunity to observe a variety of radio and plasma wave phenomena and to compare the Cassini measurements with similar instruments flown on earlier spacecraft. *Kurth et al.* [this issue] provide an overview of the RPWS observations during the flyby of the Earth. One of the primary goals for the RPWS during the flyby was to validate the wave normal and Poynting vector analysis capability of the five-channel waveform receiver (WFR). The simultaneous measurement of five components of the electric and magnetic fields by the WFR receiver allows the wave normal and Poynting vector of various low-frequency plasma waves to be determined in many cases. The wave normal vector determines the direction of propagation of a wave and is important in determining the polarization, the mode, and the source region of the wave. It can also be used to calculate the dispersion relation, to determine various resonances, to estimate the local plasma index of refraction, and to help examine wave-particle interactions. The Poynting flux determines the direction of propagation of wave energy and is also useful in determining wave modes and source-generating regions. This study will examine this capability and discuss the propagation characteristics of a variety of plasma waves.

Paper number 2001JA900114.
0148-0227/01/2001JA900114$09.00

2. Instrument Description

The RPWS consists of five receivers, a Langmuir probe, three electric antennas, and a triaxial search coil magnetometer (see D. A. Gurnett et al. (The Cassini radio and plasma wave science investigation, submitted to *Space Science Reviews*, 2000; hereinafter referred to as submitted manuscript, 2000)

for a detailed description of the instrument). The receivers cover a range from ~1 Hz to 16 MHz for electric fields and from ~1 Hz to 12 kHz for magnetic fields. This study will primarily use the five-channel waveform receiver (WFR). The WFR obtains simultaneous waveforms from up to five sensors in one of two frequency bands, either 1–26 Hz or 3 Hz to 2.5 kHz. When two electric and three magnetic antennas are used, polarization and wave normal vector measurements can be obtained, and in certain conditions, the Poynting vector can be determined. The WFR is usually operated with the E_x dipole, E_w monopole, and the three search coil magnetometers (B_x, B_y, B_z). During the period of the Earth flyby, approximately 4 hours of high-frequency filter mode data (3 Hz to 2.5 kHz) were collected, both in the solar wind and in the Earth's magnetosphere. In this high-frequency filter mode a 2048-sample waveform was captured every 20 s, with a 140-μs sample period. This produces a waveform ~0.29 s long. On September 12, 1999, while Cassini was in the solar wind, the WFR was set to the low-frequency filter mode (1–26 Hz) for approximately 2 days. During this period the WFR obtained a 2048-sample capture every 96 s. The time between samples was 0.01 s, resulting in a 20.48-s waveform.

3. Method of Analysis

In this study the Means method [*Means*, 1972], using code developed by *LeDocq* [1998] for the Polar Plasma Wave Instrument (PWI), is used to determine the wave normal vector **k**. This method involves computing a spectral matrix that consists of the autopower and cross-power spectrums from the three magnetic components. Although this method has an inherent 180° ambiguity in the wave normal direction, this ambiguity can be removed if the Poynting vector **S** can be determined. Since the wave normal vector must have a component in the direction of the energy flow, $\mathbf{S} \cdot \mathbf{k}$ must be greater then 0. Because the Cassini WFR only measures five components of electromagnetic waves (two electric and three magnetic), the Poynting vector cannot be determined directly. However, *Shawhan* [1970] showed that for electromagnetic waves below the electron cyclotron frequency, f_{ce}, the missing component can usually be estimated from the five measured components, and the Poynting vector can be determined with good accuracy using $\mathbf{S} = (1/2)\ \mathrm{Re}\{\mathbf{E}(f) \times \mathbf{H}^*(f)\}$, where the asterisk indicates the complex conjugate, Re is the real part, and $\mathbf{E}(f)$ and $\mathbf{H}(f)$ are the Fourier transforms of the electric and magnetic field waveforms.

The procedure to perform the above analysis is as follows. First, since the E_w antenna is not aligned with the z axis of the spacecraft (see D. A. Gurnett et al. (submitted manuscript, 2000) for a description of the orientation of the RPWS antennas), the three magnetic components are rotated into the coordinate system defined by the E_w monopole and E_x dipole antennas. Then the missing electric component is calculated, and all six components are rotated back into the spacecraft x,y,z coordinate system. The wave normal and Poynting vector is calculated and then transformed into a coordinate system in which the z axis is aligned with the local magnetic field (as determined by the Cassini magnetometer). Once computed, the polar θ and azimuth ϕ angles of the two vectors are displayed on a conventional frequency-time spectrogram, with $\theta = 0°$ aligned with the local field and $\phi = 0°$ defined as outward from the Earth. To reduce the background noise that is plotted, a coherence and eigenvalue test is applied to the wave normal and Poynting data to determine when they are to be plotted. For this study a coherence value of >0.90 or >0.95 between the three magnetic field components was required for the data to be plotted (see *Means* [1972] and *LeDocq* [1998] for the definition of coherence). The eigenvalue test determines the planarity of the wave. The ratio of the largest eigenvalue of the spectral matrix to the sum of the eigenvalues, R_λ, equals $\lambda_1/(\lambda_1 + \lambda_2 + \lambda_3)$, where $\lambda_1 > \lambda_2 > \lambda_3$ [*Storey et al.*, 1991; *LeDocq*, 1998]. An eigenvalue ratio of 1 refers to a single plane wave, while a ratio of 0.33 refers to an isotropic distribution of uncorrelated waves. For this study the eigenvalue limit was set to >0.9 or >0.95 for the data to be plotted. The majority of whistler mode waves observed during the flyby satisfy these two plotting conditions. It should be noted that for this study, in each 2048-sample WFR snapshot, the analysis used a 512-sample size, with a 75% overlap as we stepped through the waveform. This results in 13 calculations of θ and ϕ for each 2048-sample (~0.29 s) snapshot.

4. Observations

Plate 1 shows a 3-hour spectrogram from the medium frequency receiver (MFR) for the period around the Earth flyby. The top panel shows the electric field spectrum obtained from the E_x dipole antenna, and the bottom panel is the spectrum obtained from the B_z search coil magnetometer. The MFR sweeps from 24 Hz to 12 kHz, with 80 frequency steps in three bands. A spectrum is obtained every 32 s, with the choice of the antenna alternating between the E_x electric antenna and the B_z magnetic antenna. See D. A. Gurnett et al. (submitted manuscript, 2000) for a more detailed description of the MFR receiver. The white line in Plate 1 shows the electron cyclotron frequency that was provided by the Cassini magnetometer team (MAG). As can be seen, a wide range of emissions was observed, both electromagnetic and electrostatic, during the flyby. Cassini encountered the bow shock at approximately 0151 spacecraft event time (SCET), as can be seen from the broadband noise that was observed by the MFR and by the jump in f_{ce} at this time. As Cassini traveled through the magnetosheath (~0150–~0225 SCET), intense bursty electromagnetic emissions are observed that have characteristics similar to lion roars. This region also contained many bursty electrostatic waves. The magnetopause was encountered at approximately 0225 SCET. Chorus is observed on the outbound trajectory from about 0350 to 0415 SCET and on the inbound part from about 0229 to 0238 SCET. Plasmaspheric hiss is observed from about 0300 to 0340 SCET. The broadband burst from 0250 to 0254 SCET is interference from the sounder and is not a natural emission. This wide range of emissions provides a unique opportunity to exercise the Cassini WFR receiver and to determine the ability of the RPWS instrument to calculate the propagation characteristics of plasma waves. For this paper the propagation characteristics of the electromagnetic waves observed in the magnetosheath, magnetosphere, and the plasmasphere during the Earth flyby will be examined.

5. Whistler

Whistlers are well-known electromagnetic emissions that were first detected during World War I by *Barkhausen* [1919]. During the 1930s the dispersive properties [*Eckersley*, 1935] and the possibility of lightning being the source [*Barkhausen*, 1930] of the whistlers were investigated. However, it was not

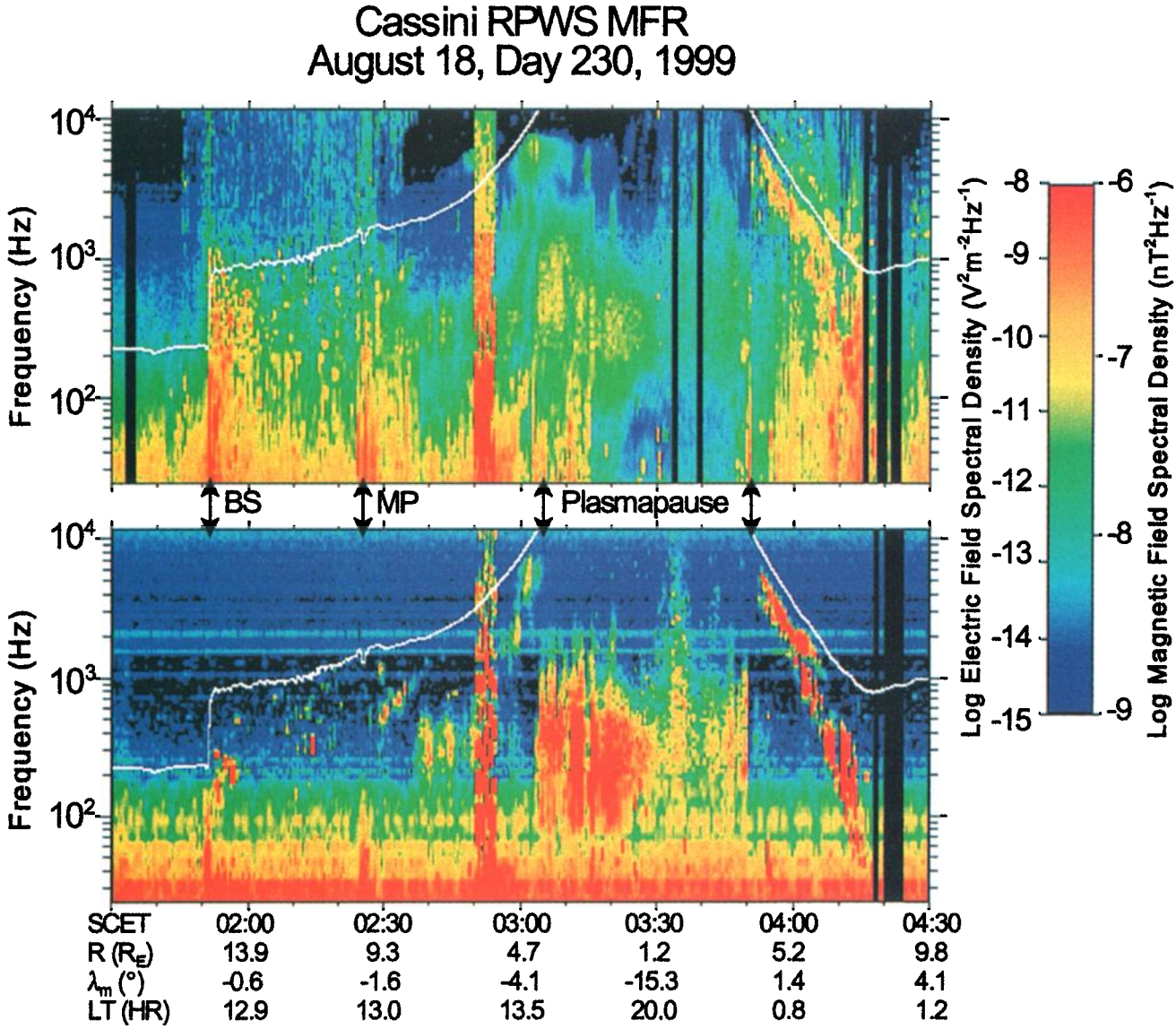

Plate 1. An overview of the magnetic and electric field spectrum observed by the Cassini radio and plasma wave instrument (RPWS) medium frequency receiver (MFR) during the Earth flyby. The crossings of the bow shock, magnetopause, and plasmapause are indicated at the bottom of the plate.

until the 1950s that *Storey* [1953] developed a theory that showed that lightning could produce the whistlers and explained the long durations of the signals which were observed. This theory, confirmed by later studies [*Helliwell et al.*, 1958; *Norinder and Knudsen*, 1959; *Helliwell*, 1965; *Walker*, 1976; *Weidman et al.*, 1983; *Carpenter and Orville*, 1989], showed that a lightning stroke produces a burst of broadband electromagnetic radiation. Some of this radiation can escape to the plasmasphere and travel along closed field lines from one hemisphere to the other in the right-hand-polarized whistler mode of propagation. Because of the anisotropy introduced by the magnetic field, the wave energy is confined to a cone that makes an angle of 19°28′ with respect to the local magnetic field. The characteristic spectrum of a whistler is a tone decreasing rapidly in frequency over a few seconds. This spectrum results because the group velocities of whistler mode waves are frequency-dependent, resulting in the high-frequency components arriving at the receiver first. When the resulting waveform is played over an audio system, it produces a tone that decreases rapidly in frequency over a few seconds.

The well-known properties of lightning-generated whistlers make them a good emission to check the calculation of the wave normal and Poynting vector and to verify the calibration of the sensors. Because of the short duration of a whistler and the low-duty cycle of the WFR during the Earth flyby, the wideband (WBR) receiver (D. A. Gurnett et al., submitted manuscript, 2000) was used to determine when whistlers were present. The periods in which whistlers were detected in the WBR were then compared with the periods that WFR data were obtained. One intense whistler was captured by the WFR in the 0327:37.706 SCET WFR snapshot. Plate 2a shows a 1-min spectrum from the WBR receiver. The broadband emission observed at approximately 0327:36 SCET is a sferic from a lightning stroke. A whistler with its characteristic falling frequency spectrum is first observed approximately 0.75 s later. The WFR snapshot occurred at 0327:37.706 SCET and is shown by the black line at the bottom of Plate 2a. The whistler in the WBR spectrum at the time of the WFR capture is observed at a frequency of approximately 2.7 kHz.

The results of the wave normal and Poynting vector determination of the whistler are shown in Plate 2b. The top two panels of Plate 2b show the sum of the electric and magnetic field spectral density, with intensity indicated by the color bar to the right. The frequency range has been set from 2 to 3.5 kHz to emphasize the whistler, which is the narrowband emission that starts at about 2.9 kHz and drifts down to about 2.4 kHz at the end of the WFR snapshot. The third panel shows the angle θ_k between the wave normal vector and the local magnetic field (10-s averaged magnetic field data), with the color bar denoting angular values ranging from 0° to 180°. As discussed above, the propagation characteristics plotted in the bottom three panels are only displayed when the coherence and eigenvalue ratio between the three magnetic components exceeds a selected value. For this example the coherence and eigenvalue ratio limits were both set at 0.90. The fourth panel shows the angle θ_s between the Poynting vector and the ambient magnetic field, with the color bar denoting angular values ranging from 0° to 180°. The fifth panel shows the sign of the z component of the Poynting vector, $S_z = \mathbf{S} \cdot \mathbf{B}_o$, where $\mathbf{B}_o$ is a unit vector parallel to the magnetic field. When S_z is positive, the Poynting vector has a component in the $+\mathbf{B}_o$ direction, and the emission is plotted in red. When S_z is negative, the Poynting vector has a component in the $-\mathbf{B}_o$ direction, and the emission is plotted in green. Both the wave normal vector and the Poynting vector are aligned nearly antiparallel to the ambient magnetic field. The average wave normal angle θ_k for this snapshot is 164 ± 6°, and the average Poynting vector angle θ_s is 169 ± 7.0°. As expected, the Poynting vector of the whistler is well within the 19°28′ cone around the magnetic field line that is required for whistler mode waves with frequencies much less than f_{ce}. The analysis also shows that the whistler is right-hand polarized. These results agree very well with whistler wave normal and Poynting vector measurements by earlier spacecraft.

The sferic observed by Cassini at 0327:36.3 SCET was also detected by the Stanford VLF group at Palmer Station, Antarctica. An analysis of the propagation characteristics of the sferic at Palmer Station suggests that the lightning stroke that produced it was in the direction of Cassini. Figure 1 shows the arrival bearing of the sferic at Palmer Station, with the star showing the location of Cassini at this time. Since the whistler detected by Cassini is traveling antiparallel to the magnetic field (southward), Cassini is observing a whistler that either originated north of Cassini or that has been reflected from the Northern Hemisphere.

6. Chorus

Chorus is one of the most intense and common emissions in the Earth's magnetosphere [*Storey*, 1953; *Allcock*, 1957; *Helliwell*, 1969]. Early spacecraft observations showed that chorus is usually observed just outside the plasmapause, ranging from L values of about 3–8, with peak intensities at about $L = 5$ [*Gurnett and O'Brien*, 1964]. Chorus ranges in frequency from a few hundred hertz to a few kilohertz and often contains complicated fine structure including rising and falling tones and short impulsive bursts [*Burtis and Helliwell*, 1969; *Dunckel and Helliwell*, 1969; *Burton and Holzer*, 1974; *Cornilleau-Wehrlin et al.*, 1978; *Hayakawa et al.*, 1990; *Sazhin and Hayakawa*, 1992; *Lauben et al.*, 1998; *LeDocq et al.*, 1998, and references therein]. Chorus is often observed during periods of disturbed magnetospheric conditions [*Tsurutani and Smith*, 1974, 1977; *Tsurutani et al.*, 1979; *Inan et al.*, 1992; *Lauben et al.*, 1998], and the occurrence of chorus is associated with energetic (10–100 keV), anisotropic ($T_\perp/T_\parallel > 1$) electron clouds [*Burton*, 1976; *Anderson and Maeda*, 1977; *Tsurutani et al.*, 1979; *Isenberg et al.*, 1982; *Sazhin and Hayakawa*, 1992]. This association between the particles and the chorus is consistent with a cyclotron resonance interaction generating the waves within regions where the static magnetic field has minimal inhomogeneities [*Kennel and Petschek*, 1966; *Curtis*, 1978; *Isenberg et al.*, 1982; *Sazhin and Hayakawa*, 1992]. Hence the magnetic equator is the most likely region for the chorus generation.

Chorus often appears in two bands, separated by a gap at one half the equatorial electron cyclotron frequency, f_{ce}, of the magnetic field line passing through the observing point [*Tsurutani and Smith*, 1974; *Burtis and Helliwell*, 1976; *Goldstein and Tsurutani*, 1984]. This dependence on f_{ce} at the equator, and the lack of dependence of the local f_{ce}, provides indirect evidence of an equatorial generation region. *Tsurutani and Smith* [1977] showed that the most intense chorus occurred at the magnetic equator, which provides additional evidence of an equatorial source region.

Various studies have examined the propagation characteristics of the chorus emissions. *Burton and Holzer* [1974] provided

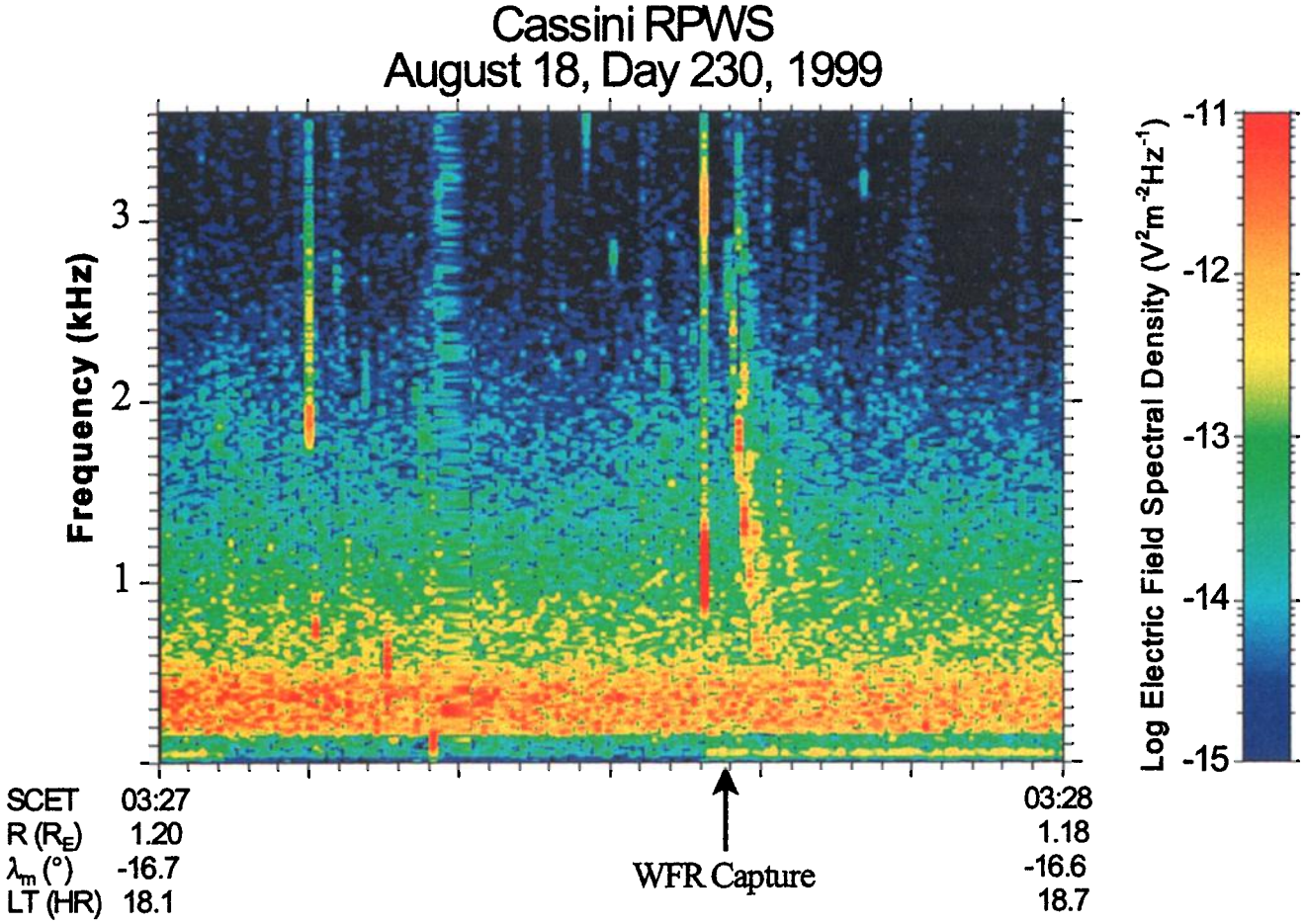

Plate 2a. Frequency-time spectrum of a whistler captured by the wideband receiver. A whistler with its characteristic falling frequency spectrum is observed to start before 0327:38 spacecraft event time (SCET). The waveform receiver (WFR) snapshot occurred at 0327:37.706 SCET and is shown by the black line at the bottom of the plate.

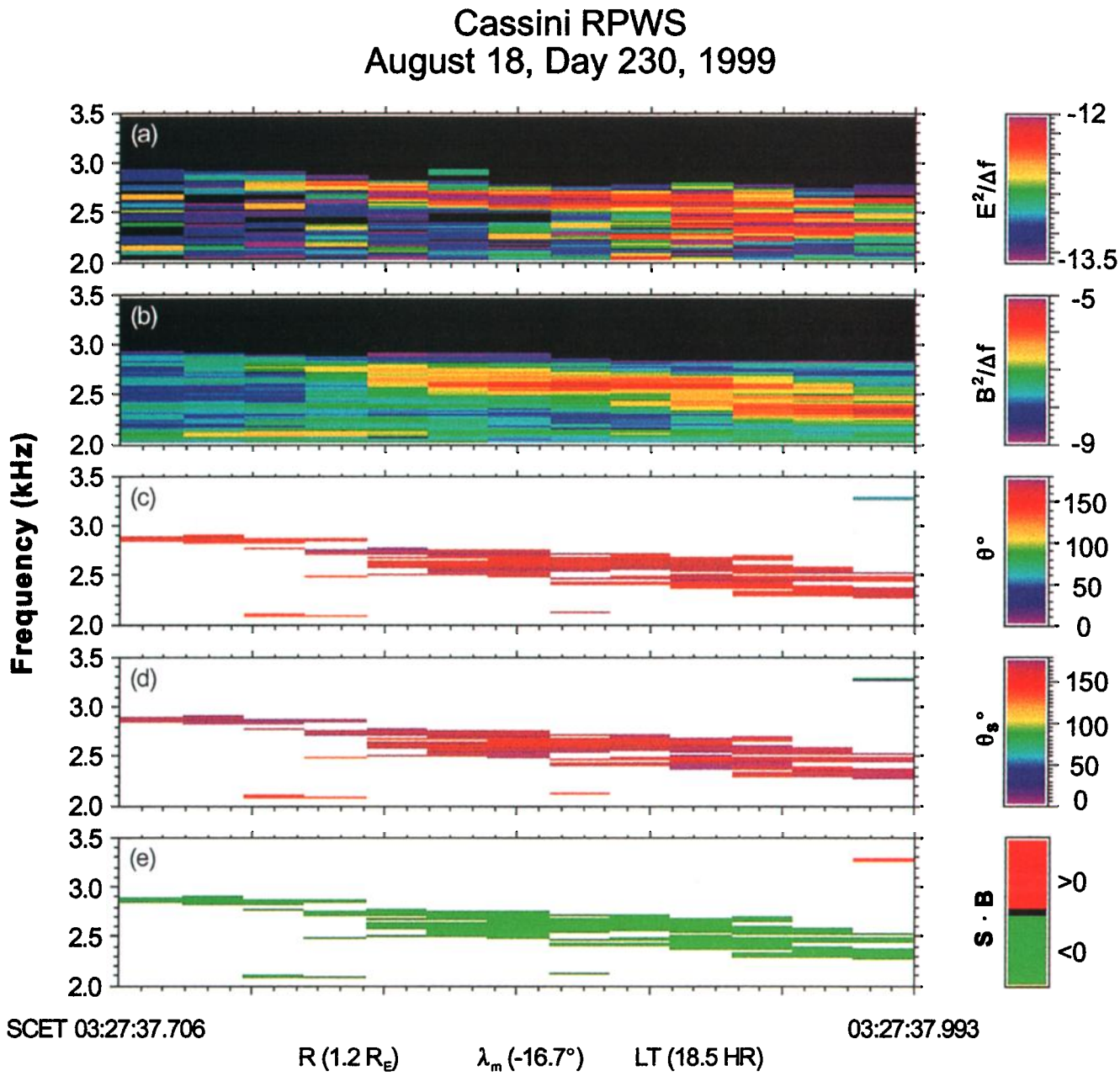

Plate 2b. A summary of the wave normal and Poynting vector direction of the whistler. The whistler is the narrowband emission that starts at about 2.9 kHz and drifts down to about 2.4 kHz at the end of the snapshot. Both the wave normal vector and the Poynting vector are aligned nearly parallel with the ambient magnetic field. The average wave normal angle, θ_k, for this snapshot is 164° ± 6°, and the average Poynting vector angle, θ_s, is 169° ± 7°.

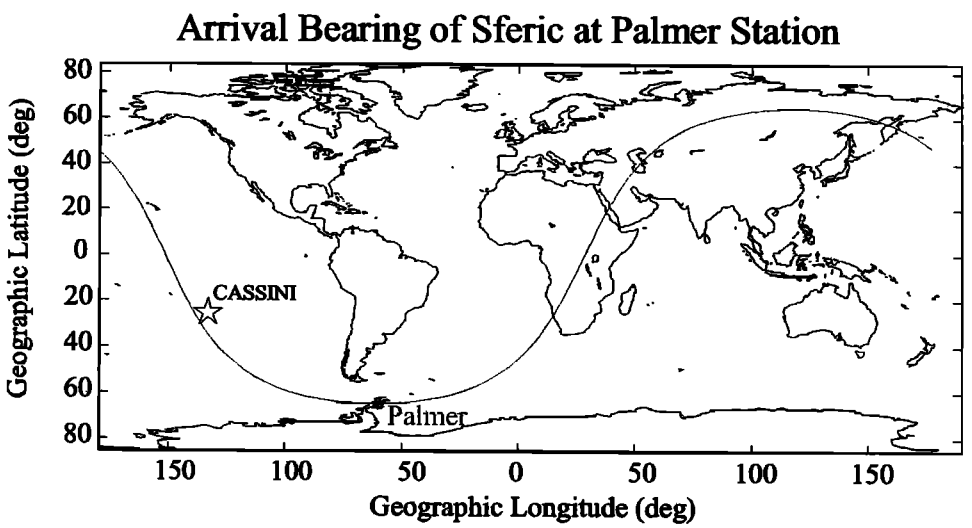

Figure 1. The arrival bearing of the sferic as determined at Palmer Station, Antarctica.

the first wave normal angle θ_k measurements of chorus and found using OGO 5 search coil data that the wave normal angles measured relative to the magnetic field were symmetrically distributed around $\theta_k = 0°$ for magnetic latitudes near the equator (<2.5°). For locations at higher latitudes, θ_k shifted to larger values, implying that the source region was within a few degrees of the magnetic equator. *Goldstein and Tsurutani* [1984] presented further OGO 5 data at locations within 5° of the magnetic equator at L shell of 6–7 and found average values of $\theta_k = 12.2°$. Near-equatorial measurements from the geostationary GEOS 2 spacecraft [*Hayakawa et al.*, 1984] at $L \approx 6.6$ found that the lower band chorus ranged from $\theta_k = 5°$–$20°$ for typical rising tone chorus. For larger df/dt rising tones, larger values of $\theta_k = 30°$–$40°$ were measured. The upper band chorus was found to have wave normal angles near the oblique resonance cone, with some variation depending on the characteristics of the fine structure of the chorus. *Muto et al.* [1987] combined off-equatorial (~17°) wave normal measurements of chorus from the GEOS 1 spacecraft and ray-tracing results to show that the equator is a possible generation region for the upper band chorus. *Muto and Hayakawa* [1987] interpreted the wave normal dependence of the upper band chorus as consistent with a generation region near the magnetic equator. Using the five-component wave field measurements (three magnetic, two electric) from the Geotail spacecraft, *Nagano et al.* [1996] presented wave normal and Poynting vector results which were consistent with generation near the magnetic equator, although some emissions were observed to propagate toward the equator. *LeDocq et al.* [1998] for the first time measured simultaneously all six components of the electric and magnetic field of chorus at a very high rate with the Polar spacecraft. From these measurements it was determined that the chorus observed by Polar was propagating away from the equator, implying that it is generated very close to the magnetic equator.

The path of Cassini during the flyby was very near the magnetic equator ($\lambda_m < 5°$) for most of the period when the spacecraft was in the magnetosphere. This location is good for examining the source region of the chorus. During the outbound part of the Cassini flyby, a series of intense chorus emissions were observed, starting at approximately 0355 SCET (see Plate 1). The spacecraft was very near the magnetic equator at this time and had just exited the plasmasphere. As the spacecraft traveled away from the Earth, the frequency at which the chorus was observed decreased. The expected gap between the two bands of chorus at ~$0.5 f_{ce}$ is easy to see in the bottom panel (B_z search coil) of Plate 1 and in Plate 3b. Plate 3 shows the results of the wave normal and Poynting vector determination of this chorus in a format similar to Plate 2b.

Plates 3c and 3d show that the wave normal and the Poynting vectors of the chorus are nearly aligned with the local magnetic field for most of this event. A closer examination also shows that the calculated Poynting vector lies within the expected 19°28′ of the local magnetic field for a whistler mode wave. The periods where there is some scatter in the calculated Poynting vector angles may be caused by the calculation of the missing electric field component. The presence of strong electrostatic emissions during an observation can affect the determination of the Poynting vector, since the missing component is determined from the measurements of the other two electric components. Although it is not shown in Plate 3, the analysis also showed that the chorus is right-hand polarized. Plates 3d and 3e show that the chorus is primarily propagating parallel to the local magnetic field (northward) for the first part of this period, with the direction changing to antiparallel (southward) in the latter half of this period. This change in the direction of propagation suggests that Cassini passed through (or near) the source region of the chorus. The magnetic latitude values shown at the bottom of Plate 3 show that Cassini was near the predicted magnetic equator during this period and suggest that Cassini should be north of the source region if the source region is at the magnetic equator. However, these values of the magnetic latitude were calculated from a simple dipole model of the Earth's magnetic field and may not be as accurate at this larger distance from the Earth. In an attempt to better understand the location of Cassini with respect to the magnetic equator during this period, the magnetic field measured by the MAG instrument was examined. Plate 3f shows the B_x (GSM) component of the magnetic field as measured by MAG. As can be seen, the B_x component goes from negative to a positive value at about 0405 SCET. Since Cassini is located at about

0100 LT, the sign of the B_x component of the magnetic field is expected to change from negative to positive very near the magnetic equator. The period of the change in sign of B_x is also the period where the chorus is observed to "flip" direction. This change in direction of the chorus such that the chorus is propagating away from the measured magnetic equator is in good agreement with the results of *LeDocq et al.* [1998].

Plate 4 shows a brief (10 min) period of emissions which appears to be chorus observed as Cassini entered the magnetosphere (Cassini crossed the magnetopause at approximately 0225 SCET). Two bands of electromagnetic emissions, the upper at about 1.1 kHz and the lower starting at about 400 Hz and rising to about 1 kHz, are observed in Plate 1 and Plate 4, starting at about 0229 SCET. An examination of the wideband data during this period shows rising tone structure that is consistent with chorus. Further evidence that these emissions are chorus is the gap between the two bands at approximately 0.5 f_{ce}. The upper band of chorus is observed for approximately 2 min, with the lower band lasting approximately 7 min. The results of the wave normal and Poynting vector determination of this chorus are shown in Plate 4. The wave normal and Poynting vector of the upper band of chorus are strongly aligned with the magnetic field in the parallel direction. The lower band is much more sporadic than the chorus observed during the outbound period, and the eigenvalue ratio tends to be lower, resulting in the limited amount that is plotted in Plate 4. The lower eigenvalue ratio indicates that two or more plane waves are present [*Storey et al.*, 1991]. The lower band of chorus plotted in Plate 4 (eigenvalue ratio greater than 0.9) is primarily aligned antiparallel to the magnetic field. The magnetic latitude determined from a dipole model suggests that Cassini is south of the magnetic equator and that the chorus is propagating both toward (upper band) and away (lower band) from the equator. An examination of the B_x (GSM) component of the measured magnetic field (Plate 4f) suggests that Cassini may be slightly north of the magnetic equator ($B_x < 0$). The location of Cassini with respect to the magnetic equator is not as well defined as in the outbound period. However, as Cassini travels southward, the chorus is observed to go from northward to southward propagation.

The most likely explanation for the chorus to be propagating both toward and away from the equator is that Cassini is passing through, or very near, the source region during these periods. Cassini was always within ~3° of the magnetic equator (as determined from a dipole model) when chorus was observed, well within the region that previous studies have predicted the generation region to be. The regions where Cassini observes the chorus propagating toward the equator are at reasonably large values of R_E (primarily at $R_E > 6$). Previous work has suggested that the source region of the chorus covers a wider range of magnetic latitude around the equator at larger R_E [see, e.g., *Tsurutani and Smith*, 1977, Figure 14; *Lauben et al.*, 2001]. Furthermore, the change in direction from one snapshot to the next on short timescales (see the lower band in Plate 3 at approximately 0406–0407 SCET) suggests that Cassini is passing near the source region, and the examination of the measured magnetic field shows that Cassini is very near the magnetic equator at this time. The difference in direction of the upper and lower bands in Plate 4 suggests that the upper and lower bands of the chorus have separate source regions and possibly a separate generation mechanism.

7. Low-Frequency Electromagnetic Emissions (Lion Roars)

Intense, bursty, narrowband electromagnetic emissions in the magnetosheath were first reported by *Smith et al.* [1969]. These emissions are usually observed in a frequency range of 0.01–0.75 f_{ce} and have a duration of from one to a few seconds. These emissions are often called "lion roars" because of their audio characteristics, which sound like a roaring lion when played on an audio system [*Smith et al.*, 1971; *Smith and Tsurutani*, 1976]. *Smith and Tsurutani* [1976] found that the waves are right-hand circularly polarized whistler mode waves, propagate nearly parallel to the ambient magnetic field, and had typical amplitudes of 0.04–0.16 nT. *Thorne and Tsurutani* [1981] showed that lion roars were related to anisotropic magnetosheath electrons ($T_{e\perp} > T_{e\parallel}$), where $T_{e\perp}$ and $T_{e\parallel}$ are the perpendicular and parallel electron temperature, and could be generated by the electron cyclotron instability. A strong relationship between the presence of lion roars and a decrease of the ambient magnetic field (usually related to mirror mode waves) has also been found [*Smith and Tsurutani*, 1976; *Tsurutani et al.*, 1982]. Various studies have suggested that temperature anisotropic electrons associated with the mirror mode waves play a role in the generation of the lion roars [*Tsurutani et al.*, 1982; *Lee et al.*, 1987; *Song et al.*, 1991, 1992], and *Chisham et al.* [1998] using Active Magnetospheric Particle Tracer Explorers (AMPTE) data confirmed the existence of anisotropic electrons inside mirror mode waves.

Using Geotail waveform data, *Zhang et al.* [1998] found two types of lion roars. The first (their type A) are associated with mirror mode waves or the decrease of the ambient magnetic field and make up about 30% of the lion roars observed in their study. The second type (their type B) were not associated with a local decrease in the ambient magnetic field. Using the minimum variance (principle axis) method, they determined the wave normal vector **k** orientation of the lion roars. The typical angle between the wave normal vector and the ambient field was ~10°, and most of the observed waves traveled in only one direction (either nearly parallel or antiparallel to the ambient magnetic field. They also found that about 5 percent of the type B lion roars had wave normal vectors in two directions and suggested that in these cases, Geotail was near the source region of the waves. A few of the type B emissions had θ_k near 90°, which they proposed may be the downstream propagating whistlers from the bow shock. *Baumjohann et al.* [1999] examined waves between the ion cyclotron and lower hybrid frequencies (frequencies lower than most of the earlier studies) in the equatorial dayside magnetosheath with the equator-S magnetometer. These emissions, which they reported as lion roars, were found in troughs of magnetosheath mirror mode waves. The waves typically lasted a few wave cycles (~0.25 s), were found to be near-monochromatic right-hand circular polarized with amplitudes of 0.2–1 nT, and were typically observed between 0.05 and 0.15 f_{ce}. The wave normal angles of these waves were found to be essentially parallel to the ambient magnetic field ($\theta_k \approx 0.3°$).

Plate 5 shows the 19-min period during which Cassini observed bursty emissions while in the magnetosheath in a format similar to Plate 2b. It should be noted that the duty cycle of the WFR during this period was rather low (a ~0.29 s waveform every 20 s). Because of this limited duty cycle, and the method by which the plotting program fills in the gaps between the

WFR captures, the bursty emissions in Plate 5 appear to occur for a longer period than they actually do. These emissions show a variety of characteristics, including a wide range of occurrence frequencies (~150 to ~700 Hz), and a large range in the ratio of the frequency of the emission to the electron cyclotron frequency (f/f_{ce} = 0.19–0.75). The waves are shown to propagate both parallel and antiparallel to the magnetic field (Plate 5f), and all were found to be right-hand polarized. Each of the 51 waveforms captured during this period was examined individually to determine if an electromagnetic emission was present. If an electromagnetic emission was present, then the propagation characteristics of the waves were determined. Of the 51 waveforms, 21 contained electromagnetic emissions that satisfied the eigenvalue and coherence test (values >0.95). Many of these 21 snapshots also contained strong electrostatic emissions near the same frequency of the electromagnetic emissions. The propagation characteristics of these waves and the effect on the analysis from the electrostatic waves are discussed below.

Plate 6 shows the propagation characteristics in a format similar to Plate 2b of one of these emissions as Cassini was approaching the magnetopause. This snapshot started at 0210: 17.736 SCET and is 0.28672 s long. The emissions are easily observed from about 400 to 550 Hz. The ratio of f/f_{ce} is ~0.5 for this event. From Plates 6c and 6e it can be seen that the wave normal vector angle θ_k and Poynting vector angle θ_s both lie nearly antiparallel to the local magnetic field. This is more easily seen in Figure 2, where θ_s and θ_k are shown on a polar plot. The top panel of Figure 2 shows the Poynting vector angles θ_s, and the bottom panel shows the wave normal vector angles θ_k. The radius of the plots is frequency, from 300 to 600 Hz, and the circumference is angle, from 0° to 180°. The average values for this snapshot are θ_s = 156° ± 13° and θ_k = 173° ± 5°. The wave normal azimuthal angles ϕ_k, shown in Plate 6d, are scattered over the 360°, with a small preference in the directions 180° and 360°. These values for the angles with respect to the magnetic field, and the fact that these waves are right-hand polarized (not shown), are consistent with these emissions propagating in the whistler mode.

Figure 3 shows the wave normal and Poynting vector angles (θ_s and θ_k) for a snapshot that occurred at 0207:37.737 SCET, approximately 3 min earlier than the example shown in Plate 6 and Figure 2. The emissions are observed at approximately 550–600 Hz, and the ratio f/f_{ce} is ~0.6. Figure 3 shows that both θ_s and θ_k are centered around ~20° for the entire frequency range of this emission. The average value of θ_s is 21° ± 8°, and θ_k is 20° ± 5°. These waves are propagating in the opposite direction (parallel to the local magnetic field) of the emission shown in Plate 6 and Figure 2. These waves are also right-hand polarized and are consistent with propagation in a whistler wave mode.

Figure 4 shows the values of the Poynting and wave normal angles from a snapshot near the beginning of this interval (0154:17.743 SCET), not long after the spacecraft entered the magnetosheath. The emissions of interest are the narrowband emissions from about 150 to 240 Hz ($f/f_{ce} \approx 0.2$). Unlike the examples in Figures 2 and 3, this emission shows the Poynting vector for this period to be nearly perpendicular to the local magnetic field, with an average value for θ_s of 77° ± 19°. This large value for θ_s is not consistent with a whistler mode wave since the angle is greater than 19°. Although it is possible that we are seeing a different wave mode, it is more likely that this is not an accurate representation of the Poynting vector direction of the electromagnetic emissions. As discussed above, Cassini only measures two components of the electric field, and the missing component is calculated from the five measured electric and magnetic components. During this snapshot (and many of the other snapshots during this early period in the magnetosheath), strong electrostatic emissions are observed in the E_x and E_w channels of the WFR, often with frequencies near the frequency of the electromagnetic emission (see Plate 5a). Furthermore, the electromagnetic emission is rather weak during this snapshot. These two conditions may result in an inaccurate determination of the missing electric field component and therefore result in an inaccurate determination of the Poynting vector.

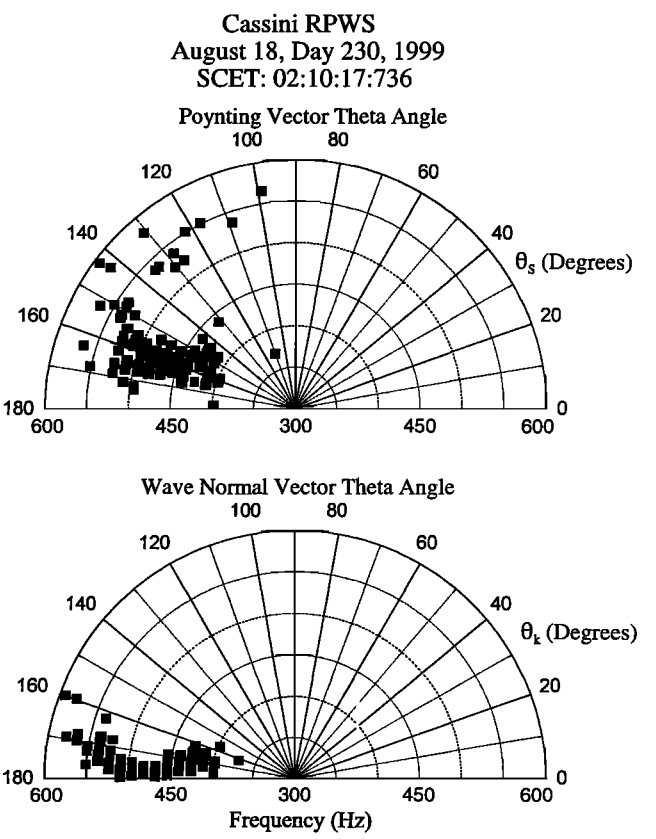

Figure 2. A summary of the θ angles between (top) the Poynting and (bottom) wave normal vector, and the local magnetic field for the emission shown in Plate 6. The radius of the plots is frequency, from 300 to 600 Hz, and the circumference is angle, from 0° to 180°. The average values for this period are θ_s = 156° ± 13° and θ_k = 173° ± 5°.

The fact that θ_s appears to be scattered around 90° also impacts the determination of the direction of the wave normal vector. The bottom panel of Figure 4 shows that the wave normal vectors for this example appear to be pointing both parallel and antiparallel to the local magnetic field. The reason for the two apparent wave normal angle values shown in Figure 4 is the use of the Poynting vector to remove the 180° ambiguity in the Means method calculation of the wave normal vector. As discussed above, $\mathbf{S} \cdot \mathbf{k}$ must be greater than 0, and if $\mathbf{S} \cdot \mathbf{k} < 0$ in the original calculation of $\mathbf{k}$, then $\mathbf{k}$ is "flipped" ($\mathbf{k}_{new} = -\mathbf{k}_{old}$) to satisfy this requirement. During this period the initial values for θ_k as determined from the Mean method before the 180° ambiguity check are nearly parallel (~26°) to

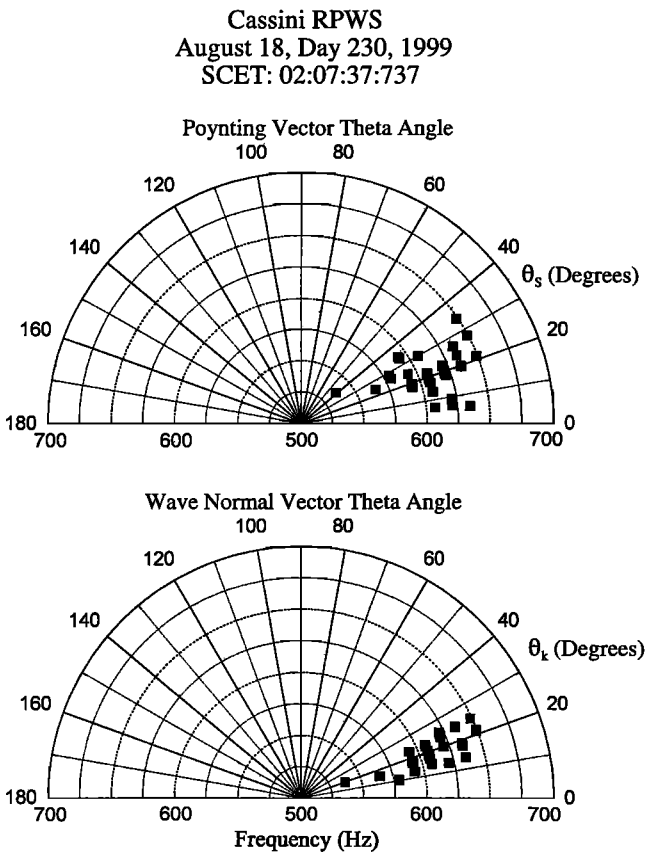

Figure 3. A summary of the θ angles between the Poynting and wave normal vector, and the local magnetic field for the emission detected at 0207:37.737 SCET. The radius of the plots is frequency, from 500 to 700 Hz, and the circumference is angle, from 0° to 180°. The average values for this period are $\theta_s = 21° \pm 8°$ and $\theta_k = 20° \pm 5°$.

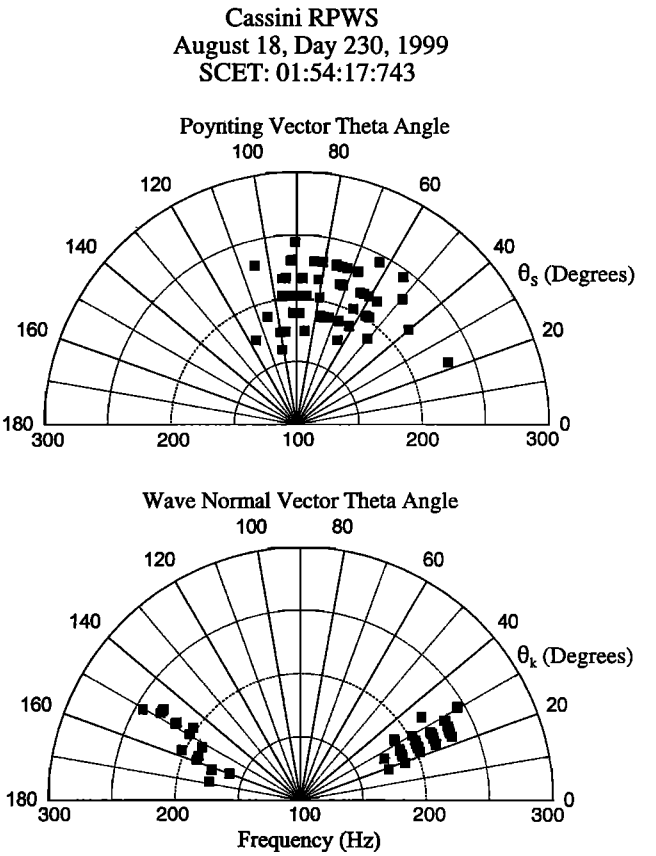

Figure 4. A summary of the angle between the Poynting and wave normal vector, and the local magnetic field for the emission detected at 0154:17.743 SCET. The radius of the plots is frequency, from 100 to 300 Hz, and the circumference is angle, from 0° to 180°. The average values for this period are $\theta_s = 77° \pm 19°$ and $\theta_k = 26° \pm 3°$; $154° \pm 7°$.

the local magnetic field. The calculation that removes the 180° ambiguity results in the $\theta_s > 90°$ measurements "flipping" the wave normal vector to the antiparallel direction. The average results for θ_k after this flipping are for $\theta_s < 90°$, $\theta_k = 26° \pm 3°$, and for $\theta_s > 90°$, $\theta_k = 154° \pm 7°$. It should be noted that uncertainty in the Poynting vector determination does not affect the "absolute" value of θ_k (26° in this example), just the determination if the vector is aligned parallel or antiparallel to the local magnetic field.

Table 1 and Figure 5 summarize the values of θ_s and θ_k for the 21 events that were detected during this period. The ratio of the center frequency of the emissions to the electron cyclotron frequency f_{ce} is also shown in Table 1. From Table 1 it can be seen that the ratio of f/f_{ce} covers a large range ($f/f_{ce} = 0.19$–0.75). The emissions tend to have ratios less than ~0.3 for the first part of the period (<~0159 SCET), and the ratios tend to increases to values greater than ~0.45 (up to 0.75) for the latter part of the period (nearer the magnetopause). These emissions cover a wide range in frequency, and no obvious gap at 0.5 f_{ce} is observed. The top panel of Figure 5 shows the values of θ_s obtained for the 21 events. At the beginning of the period (near the bow shock), θ_s appears to be around 90° with respect to the local magnetic field, while at the end of the period (near the magnetopause), θ_s tends to be more aligned with the local magnetic field. As discussed above, the values of θ_s near 90° are not expected for whistler mode waves. The presence of strong electrostatic waves in this region (see Plate 5a) may be affecting the determination of the missing electric field component, resulting in the nearly perpendicular values for the Poynting vectors. As Cassini moves away from the bow shock, the occurrence frequency and the strength of the electrostatic emissions are reduced. This may explain why the emissions detected later in this period have Poynting vectors which are more typical for whistler mode waves. For the cases where the Poynting vector is nearly aligned with the magnetic field, the waves are found to propagate both parallel and antiparallel to the local magnetic field.

The bottom panel of Figure 5 shows that the wave normal vectors in all 21 cases are nearly aligned with respect to the local magnetic field. The average wave normal angle for the 21 cases is 16°, with the largest being 38°. This average is slightly larger than the typical value of 10° for lion roars observed by Geotail [*Zhang et al.*, 1998]. An examination of the direction of the wave normal vector with respect to the local magnetic field shows that the waves are almost evenly split between parallel and antiparallel propagation (10 parallel, eight antiparallel). For the cases that showed both a direction up and down the field (caused by θ_s being scattered around 90°), if one direction dominated, it was defined as parallel or antiparallel. Three events had wave normal directions in which neither direction

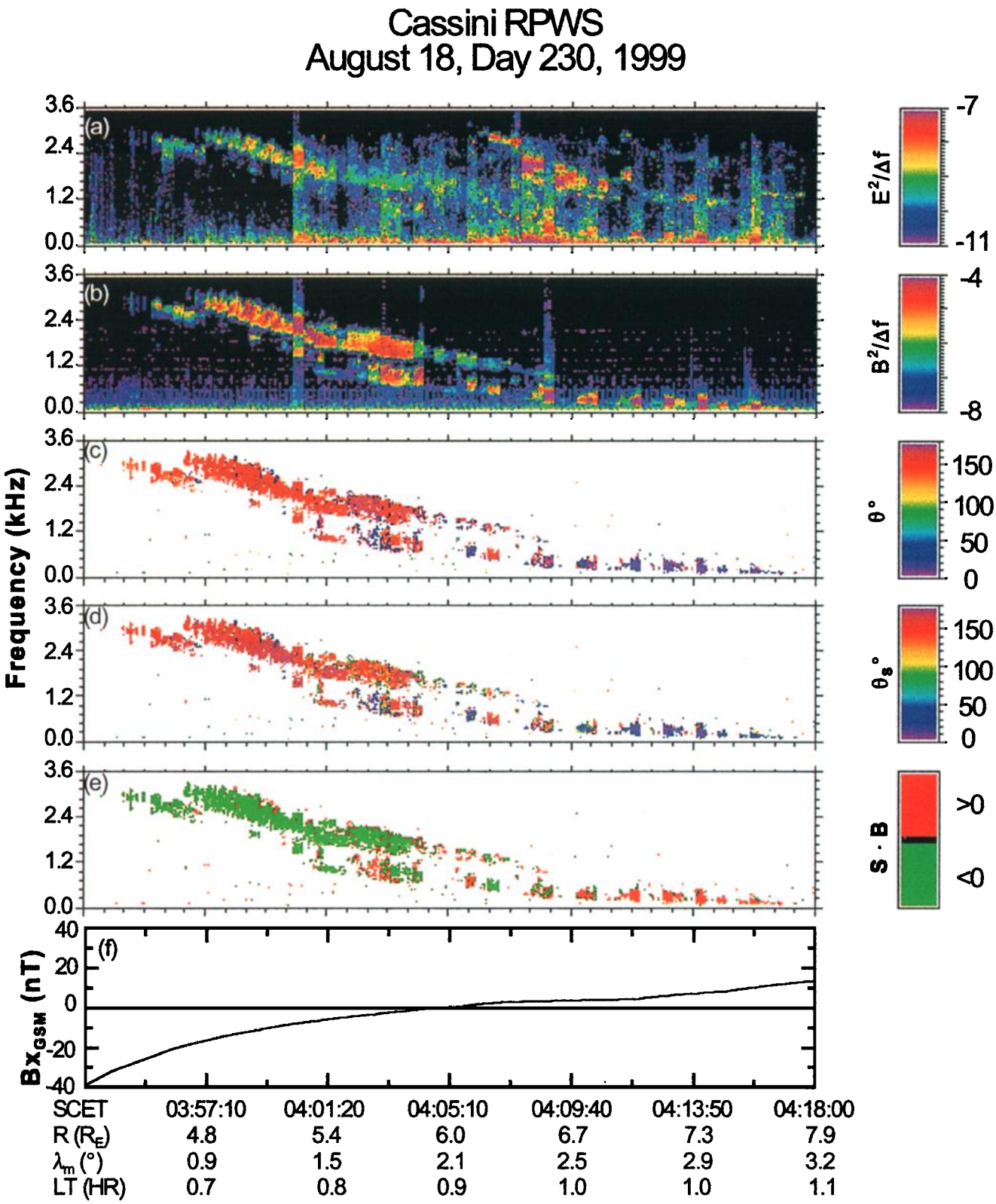

Plate 3. A summary of the WFR receiver observations of the wave normal and Poynting vector direction of the chorus emissions observed on the outbound part of the flyby.

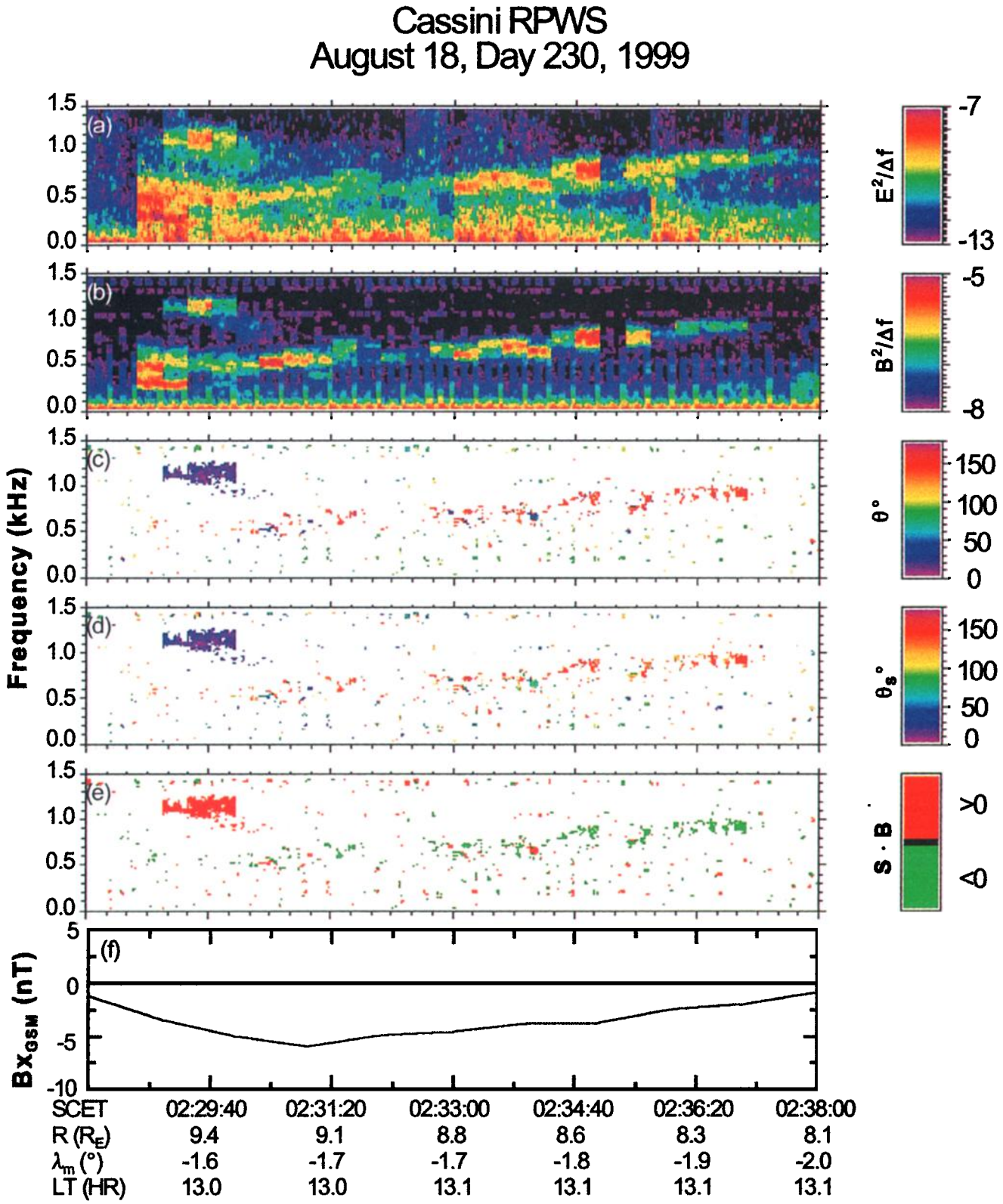

Plate 4. A summary of the WFR receiver observations of the wave normal and Poynting vector direction of chorus emissions detected during the inbound part of the flyby.

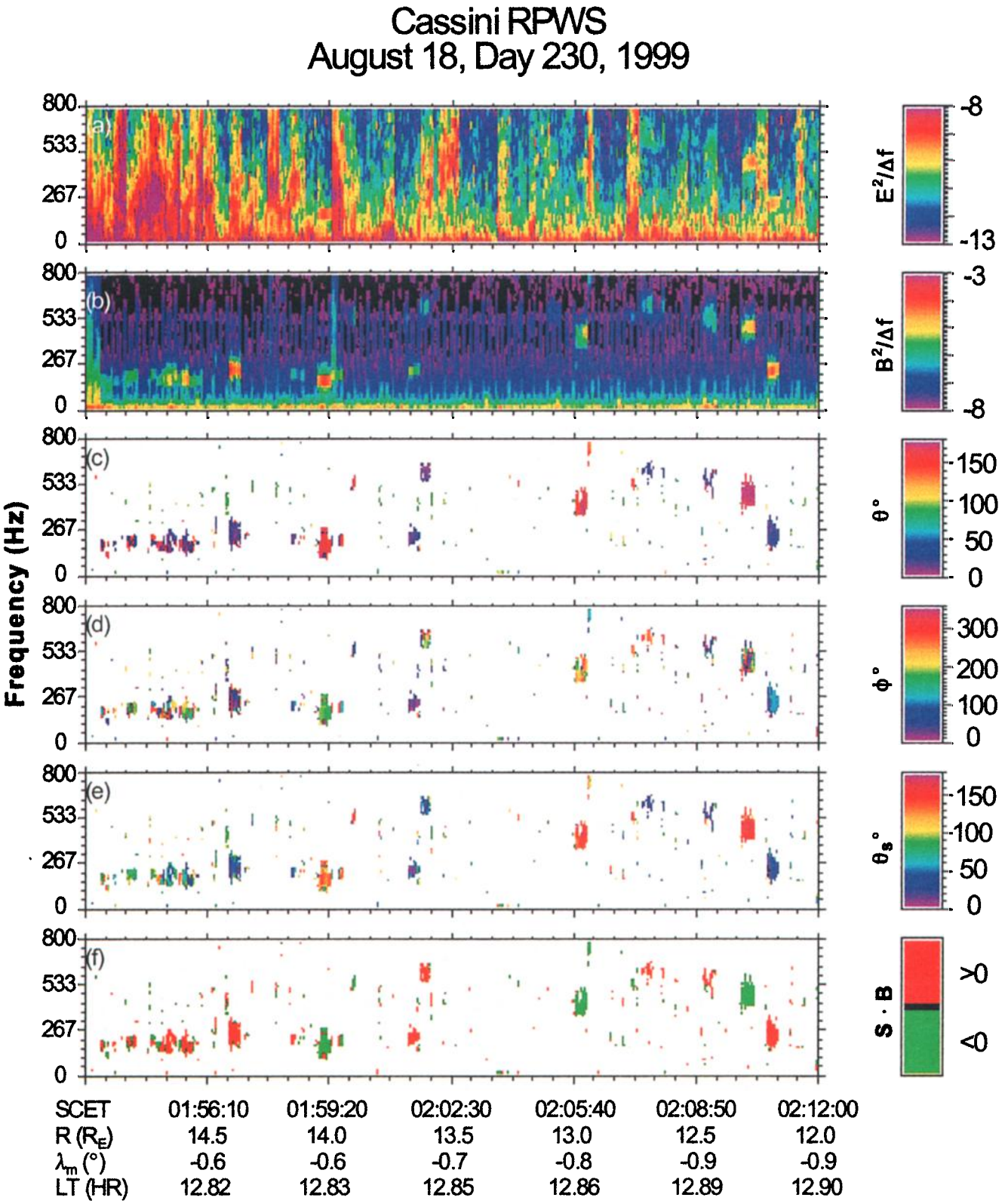

Plate 5. A summary of the WFR receiver observations of the wave normal and Poynting vector direction of low-frequency emissions in the magnetosheath.

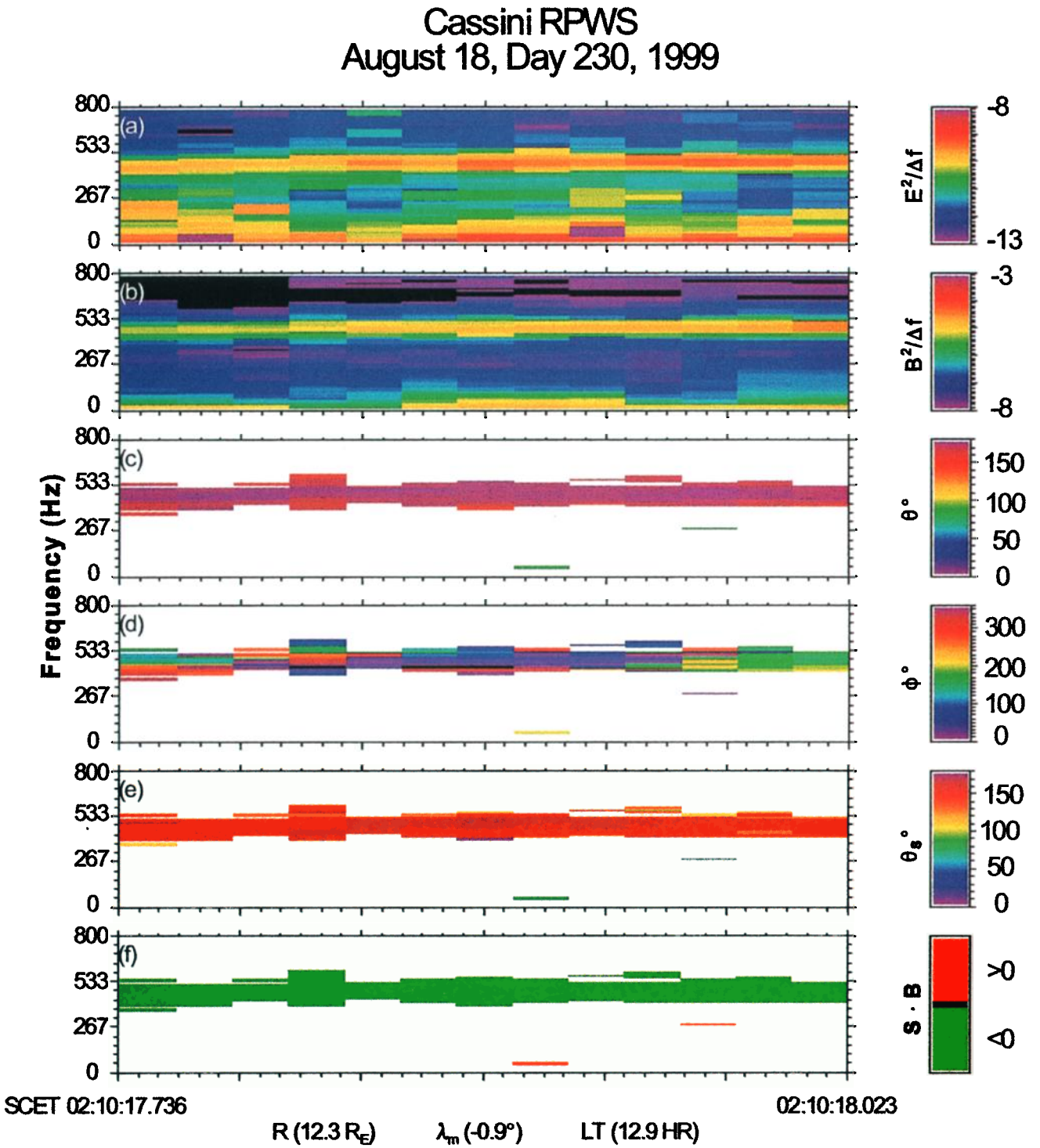

Plate 6. A summary of the WFR receiver observations of the wave normal and Poynting vector direction of the snapshot at 0210:17.736 SCET of the low-frequency emissions in the magnetosheath.

Table 1. Values for 21 Events

Spacecraft Event Time	f/f_{ce}	θ_s, deg	θ_k, deg
0154:17.7	0.23	77 ± 19	26 ± 3
			154 ± 7
0154:57.7	0.24	83 ± 29	26 ± 3
			154 ± 7
0155:17.7	0.23	62 ± 22	11 ± 6
			169 ± 5
0155:37.7	0.20	80 ± 44	11 ± 5
			169 ± 3
0155:57.7	0.19	63 ± 33	25 ± 4
			154 ± 4
0156:37.7	0.35	87 ± 18	9 ± 2
			167 ± 5
0156:57.7	0.28	40 ± 28	13 ± 6
			164 ± 8
0159:17.7	0.20	119 ± 30	19 ± 7
			163 ± 5
0159:37.7	0.23	102 ± 42	10 ± 7
			162 ± 7
0159:57.7	0.65	161 ± 9	167 ± 3
0201:37.7	0.24	24 ± 23	14 ± 6
0201:57.7	0.66	42 ± 20	9 ± 6
0204:17.7	0.60	126 ± 7	164 ± 4
0205:57.7	0.46	148 ± 11	164 ± 7
0206:17.7	0.75	126 ± 17	142 ± 12
0207:17.7	0.55	137 ± 22	156 ± 5
0207:37.7	0.62	21 ± 8	20 ± 5
0207:57.7	0.66	47 ± 14	23 ± 9
0209:17.7	0.56	26 ± 17	12 ± 6
		128 ± 11	175 ± 2
0210:17.7	0.47	156 ± 13	173 ± 5
0210:57.7	0.26	23 ± 14	169 ± 6

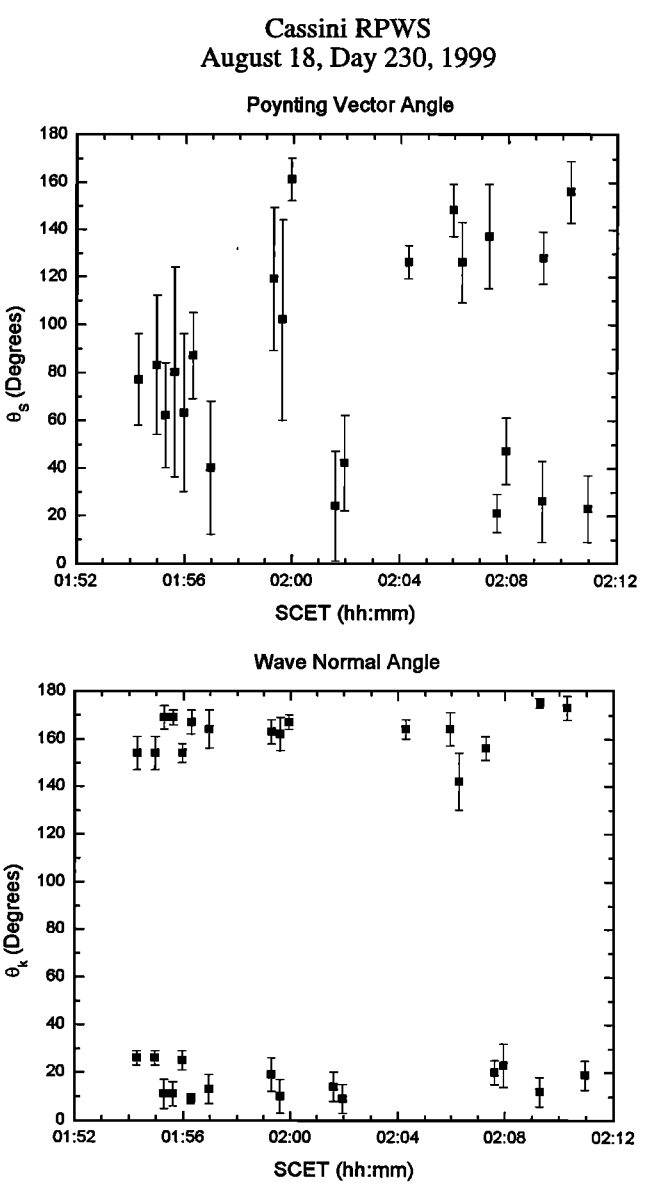

Figure 5. A summary of the angle between the Poynting and wave normal vector, and the local magnetic field for the 21 events that were observed by Cassini in the magnetosheath. The top shows that at the beginning of the period (near the bow shock), θ_s appears to be around 90° with respect to the local magnetic field, while at the end of the period (near the magnetopause), θ_s tends to be more aligned with the local magnetic field. The bottom panel shows that the wave normal vectors in all 21 cases are nearly aligned (both parallel and antiparallel) with respect to the local magnetic field. The average wave normal angle for the 21 cases is 16°.

dominated. Since the majority of the snapshots contain emissions with wave normal vectors in one direction only (assuming the θ_s scattered around 90° are not accurate), the source region for these waves is probably far from the spacecraft. Furthermore, the change in the wave normal direction between two adjacent snapshots (for example, 0207:17.7 and 0207:37.7 SCET) implies that there are multiple source regions.

Using the definitions of the "types" of lion roars from *Zhang et al.* [1998], we determine that the Cassini observations are probably a mixture of type A and type B lion roars. B. Tsurutani (personal conversation, 2001) showed that there was little or no evidence of mirror mode structures detected by the Cassini magnetometer during this period. Some of the emissions detected by the WFR do occur in regions of decreasing or minimum local magnetic field, which would correspond to *Zhang et al.* [1998] type A. However, these decreases are usually only a few to 10 percent, so it is unclear if these can be claimed to be associated with mirror mode structures. Furthermore, some of the emissions do not appear to correspond to minimums of the magnetic field (type B).

8. Conclusions

The measurements obtained during the Earth flyby provided an opportunity to validate the wave normal and Poynting vector analysis capabilities of the WFR receiver. These preliminary results are very promising. Propagation characteristics of a variety of plasma waves were determined and compared with measurements obtained from previous spacecraft. The measurement of a lightning-induced whistler agrees very well with the results of earlier spacecraft. The chorus was found to be propagating nearly aligned with the magnetic field, and the majority of the emissions were found to be propagating away from the equator, even when Cassini was very close to the magnetic equator, suggesting that the source region is very near the magnetic equator. The examination of the low-frequency emissions (lion roars) in the magnetosheath also produced agreement with earlier studies, especially with regard to the determination of the wave normal vectors using Geotail data [*Zhang et al.*, 1998]. However, these emissions also showed the limitation in calculating the Poynting vector with

only five measured components. These limitations will be examined in a future work.

Acknowledgments. The research at the University of Iowa is supported by the National Aeronautics and Space Administration through contract 961152 with the Jet Propulsion Laboratory. G. B. Hospodarsky acknowledges B. Tsurutani and O. Santolik for useful discussions.

Michel Blanc and Guest Editor Stanley Cowley thank Rudolf Treumann and another referee for their assistance in evaluating this paper.

References

Allcock, G. M., A study of the audio-frequency radio phenomenon known as "dawn chorus," *Aust. J. Phys.*, *10*, 286, 1957.

Anderson, R. R., and K. Maeda, VLF emissions associated with enhanced magnetospheric electrons, *J. Geophys. Res.*, *82*, 135, 1977.

Barkhausen, H., Zwei mit Helfe der neuen Verstärker entdeckte Erscheinungen, *Phys. Z.*, *20*, 401, 1919.

Barkhausen, H., Whistling tones from the Earth, *Proc. IRE*, *18*, 1155, 1930.

Baumjohann, W., R. A. Treumann, E. Georgescu, G. Haerendel, K.-H. Fornacon, and U. Auster, Waveform and packet structure of lion roars, *Ann. Geophys.*, *17*, 1528, 1999.

Burtis, W. J., and R. A. Helliwell, Banded chorus: A new type of VLF radiation observed in the magnetosphere by OGO 1 and OGO 3, *J. Geophys. Res.*, *74*, 3002, 1969.

Burtis, W. J., and R. A. Helliwell, Magnetospheric chorus: Occurrence patterns and normalized frequency, *Planet. Space Sci.*, *24*, 1007, 1976.

Burton, R. K., Critical electron pitch angle anisotropy necessary for chorus generation, *J. Geophys. Res.*, *81*, 4779, 1976.

Burton, R. K., and R. E. Holzer, The origin and propagation of chorus in the outer magnetosphere, *J. Geophys. Res.*, *79*, 1014, 1974.

Carpenter, D. L., and R. E. Orville, The excitation of active whistler mode signal paths in the magnetosphere by lightning: Two case studies, *J. Geophys. Res.*, *94*, 8886, 1989.

Chisham, G., D. Burgess, S. J. Schwartz, and M. W. Dunlop, Observations of electron distributions in magnetosheath mirror mode waves, *J. Geophys. Res.*, *103*, 26,765, 1998.

Cornilleau-Wehrlin, N., R. Gendrin, F. Lefeuvre, M. Parrot, R. Grard, D. Jones, A. Bahnsen, E. Ungstrup, and W. Gibbons, VLF electromagnetic waves observed onboard GEOS-1, *Space Sci. Rev.*, *22*, 371, 1978.

Curtis, S. A., A theory for chorus generation by energetic electrons during substorms, *J. Geophys. Res.*, *83*, 3841, 1978.

Dunckel, N., and R. A. Helliwell, Whistler mode emissions on the OGO 1 satellite, *J. Geophys. Res.*, *74*, 6371, 1969.

Eckersley, T. L., Musical atmospherics, *Nature*, *135*, 104, 1935.

Goldstein, B. E., and B. T. Tsurutani, Wave normal directions of chorus near the equatorial source region, *J. Geophys. Res.*, *89*, 2798, 1984.

Gurnett, D. A., and B. J. O'Brien, High-latitude geophysical studies with satellite Injun 3, 5, Very low frequency electromagnetic radiation, *J. Geophys. Res.*, *69*, 65, 1964.

Hayakawa, M., Y. Yamanaka, M. Parrot, and F. Lefeuvre, The wave normals of magnetospheric chorus emissions observed on board GEOS 2, *J. Geophys. Res.*, *89*, 2811, 1984.

Hayakawa, M., K. Hattori, S. Shimakura, M. Parrot, and F. Lefeuvre, Direction finding of chorus emissions in the outer magnetosphere and their generation and propagation, *Planet. Space Sci.*, *38*, 135, 1990.

Helliwell, R. A., *Whistlers and Related Ionospheric Phenomena*, Stanford Univ. Press, Stanford, Calif., 1965.

Helliwell, R. A., Low-frequency waves in the magnetosphere, *Rev. Geophys.*, *7*, 281, 1969.

Helliwell, R. A., A. G. Jean, and W. L. Taylor, Some properties of lightning impulses which produce whistlers, *Proc. IEEE*, *46*, 1760, 1958.

Inan, U. S., Y. T. Chiu, and G. T. Davidson, Whistler-mode chorus and morningside aurorae, *Geophys. Res. Lett.*, *19*, 653, 1992.

Isenberg, P. A., H. C. Koons, and J. F. Fennell, Simultaneous observations of energetic electrons and dawnside chorus in geosynchronous orbit, *J. Geophys. Res.*, *87*, 1495, 1982.

Kennel, C. F., and H. E. Petschek, Limit on stably trapped particle fluxes, *J. Geophys. Res.*, *71*, 1, 1966.

Kurth, W. S., G. B. Hospodarsky, D. A. Gurnett, M. L. Kaiser, J.-E. Wahlund, A. Roux, P. Canu, P. Zarka, and Y.-V. Tokarev, An overview of observations by the Cassini radio and plasma wave investigation at Earth, *J. Geophys. Res.*, this issue.

Lauben, D. S., U. S. Inan, T. F. Bell, D. L. Kirchner, G. B. Hospodarsky, and J. S. Pickett, VLF chorus emissions observed by Polar during the January 10, 1997, magnetic cloud, *Geophys. Res. Lett.*, *25*, 2995, 1998.

Lauben, D. S., U. S. Inan, T. F. Bell, and D. A. Gurnett, Source characteristics of ELF/VLF chorus, *J. Geophys. Res.*, in press, 2001.

LeDocq, M. J., Wave normal and Poynting flux directions of magnetospheric plasma waves, Ph.D. thesis, 178 pp., Univ. of Ia., Iowa City, Iowa, 1998.

LeDocq, M. J., D. A. Gurnett, and G. B. Hospodarsky, Chorus source location from VLF Poynting flux measurements with the Polar spacecraft, *Geophys. Res. Lett.*, *25*, 4063, 1998.

Lee, L. C., C. S. Wu, and C. P. Price, On the generation of magnetosheath lion roars, *J. Geophys. Res.*, *92*, 2343, 1987.

Means, J. D., Use of the three-dimensional covariance matrix in analyzing the polarization properties of plane waves, *J. Geophys. Res.*, *77*, 5551, 1972.

Muto, H., and M. Hayakawa, Ray-tracing study of the propagation in the magnetosphere of whistler-mode VLF emissions with frequency above one half the gyrofrequency, *Planet. Space Sci.*, *35*, 1397, 1987.

Muto, H., M. Hayakawa, M. Parrot, and F. Lefeuvre, Direction finding of half-gyrofrequency VL emissions in the off-equatorial region of the magnetosphere and their generation and propagation, *J. Geophys. Res.*, *92*, 7538, 1987.

Nagano, I., S. Yagitani, H. Kojima, and H. Matsumoto, Analysis of wave normal and Poynting vectors of chorus emissions observed by Geotail, *J. Geomagn. Geoelectr.*, *48*, 299, 1996.

Norinder, H., and E. Knudsen, The relation between lightning discharges and whistlers, *Planet. Space Sci.*, *1*, 173, 1959.

Sazhin, S. S., and M. Hayakawa, Magnetospheric chorus emissions: A review, *Planet. Space Sci.*, *40*, 681, 1992.

Shawhan, S. D., The use of multiple receivers to measure the wave characteristics of very-low-frequency noise in space, *Space Sci. Rev.*, *10*, 689, 1970.

Smith, E. J., and B. T. Tsurutani, Magnetosheath lion roars, *J. Geophys. Res.*, *81*, 2261, 1976.

Smith, E. J., R. E. Holtzer, and C. T. Russell, Magnetic emissions in the magnetosheath at frequencies near 100 Hz, *J. Geophys. Res.*, *74*, 3027, 1969.

Smith, E. J., A. M. A. Frandsen, and R. E. Holzer, Lion roars in the magnetosheath (abstract), *Eos Trans. AGU*, *52*, 903, 1971.

Song, P., C. T. Russell, R. J. Strangeway, and R. R. Anderson, Interrelationship between magnetosheath ULF waves and VLF waves, *Phys. Space Plasmas*, *11*, 459, 1991.

Storey, L. R. O., An investigation of whistling atmospherics, *Philos. Trans. R. Soc. London*, *246*, 113, 1953.

Storey, L. R. O., F. Lefeuvre, M. Parrot, L. Cairo, and R. R. Anderson, Initial survey of the wave distribution functions for plasmaspheric hiss observed by ISEE 1, *J. Geophys. Res.*, *96*, 19,469, 1991.

Song, P., C. T. Russell, and M. F. Thomsen, Waves in the inner magnetosheath: A case study, *Geophys. Res. Lett.*, *19*, 2191, 1992.

Thorne, R. M., and B. T. Tsurutani, The generation mechanism for magnetosheath lion roars, *Nature*, *293*, 384, 1981.

Tsurutani, B. T., and E. J. Smith, Postmidnight chorus: A substorm phenomenon, *J. Geophys. Res.*, *79*, 118, 1974.

Tsurutani, B. T., and E. J. Smith, Two types of magnetospheric ELF chorus and their substorm dependence, *J. Geophys. Res.*, *82*, 5112, 1977.

Tsurutani, B. T., E. J. Smith, H. I. West Jr., and R. M. Buck, Chorus, energetic electrons and magnetospheric substorms, in *Wave Instabilities in Space Plasma*, edited by P. J. Palmadesso and K. Papadopoulos, p. 55, D. Reidel, Norwell, Mass., 1979.

Tsurutani, B. T., E. J. Smith, R. R. Anderson, K. W. Ogilvie, J. D. Scudder, D. N. Baker, and S. J. Bame, Lion roars and nonoscillatory drift mirror waves in the magnetosheath, *J. Geophys. Res.*, *87*, 6060, 1982.

Walker, A. D. M., The theory of whistler propagation, *Rev. Geophys.*, *14*, 1629, 1976.

Weidman, C. D., E. P. Krider, C. G. Park, and B. Blockley, Correlated measurements of lightning radiation fields and whistlers, in *Proceed-*

ings in Atmospheric Electricity, edited by L. H. Ruhnke and J. Latham, p. 334, A. Deepak, Hampton, Va., 1983.

Zhang, Y., H. Matsumoto, and H. Kojima, Lion roars in the magnetosheath: The Geotail observations, *J. Geophys. Res.*, *103*, 4615, 1998.

T. F. Averkamp, D. A. Gurnett, G. B. Hospodarsky, and W. S. Kurth, Department of Physics and Astronomy, University of Iowa, Iowa City, IA 52242, USA. (george-hospodarsky@uiowa.edu)

M. Dougherty, Blackett Laboratory, Imperial College of Science and Technology, Room 6M54, Huxley Building, Prince Consort Road, London SW7 2BW, England.

U. Inan and T. Wood, Department of Electrical Engineering, Stanford University, Stanford, CA 94305, USA.

(Received November 11, 2000; revised July 23, 2001; accepted July 24, 2001.)